Power-Efficient Analog Front-End Interference Suppression With Binary Antennas

Sajjad Nassirpour[®], *Graduate Student Member, IEEE*, Agrim Gupta[®], *Student Member, IEEE*, Alireza Vahid[®], *Senior Member, IEEE*, and Dinesh Bharadia[®], *Member, IEEE*

Abstract—Digital and analog beamforming are well-known methods to suppress interference using multiple-antenna structures, but they have practical limitations: (i) Digital beamforming requires multiple analog-to-digital converters (ADCs) to enable digital conversion, which increases the cost and complexity; (ii) Although analog beamforming does not require expensive ADCs, it uses phase shifters, which cause quantization errors, insertion losses, and reduced power efficiency. In this paper, we consider a K-user uplink interference channel and propose a low-complexity algorithmic interference-suppression solution relying on simple switch-based reconfigurable antennas at the receivers. We utilize switches to enable/disable antennas to maximize each user's signal-to-interference-plus-noise ratio (SINR). We present an optimization approach to approximate the optimal solution. To evaluate the results, we compare our method with relevant benchmarks. Moreover, we derive a lower bound on the minimum number of antenna elements per receiver to attain the desired SINR and verify the findings via simulations.

Index Terms—Distributed interference suppression, reconfigurable antennas, integer programming, fading channels, throughput, channel state information.

I. INTRODUCTION

WITH upcoming technologies like base-station (BS) on drones [1], [2], [3], satellites [4], [5], [6] and mobile vehicles [7], as well as a push toward green communications to optimize the carbon footprint [8], [9], [10], the power consumption metrics of BSs ought to be optimized. Further, the deployment density of BSs increases with the next generation of wireless communications [11], [12], which demands better interference management strategies. The problem can be modeled as a K-user interference channel.

One solution is to have the BSs occupy different chunks of spectrum, which avoids any interference in the first place, but

Manuscript received 9 April 2022; revised 10 August 2022; accepted 23 September 2022. Date of publication 14 October 2022; date of current version 11 April 2023. The work of Sajjad Nassirpour and Alireza Vahid was supported in part by the National Science Foundation (NSF) under Grant ECCS-2030285, Grant CNS-2106692, and Grant CNS-2211804. The work of Agrim Gupta and Dinesh Bharadia was supported in part by the NSF under Grant CNS-1925767, Grant CNS-2107613, and Grant ECCS-2030245. The associate editor coordinating the review of this article and approving it for publication was S. Zhou. (Corresponding author: Sajjad Nassirpour.)

Sajjad Nassirpour and Alireza Vahid are with the Department of Electrical Engineering, University of Colorado Denver, Denver, CO 80204 USA (e-mail: sajjad.nassirpour@ucdenver.edu; alireza.vahid@ucdenver.edu).

Agrim Gupta and Dinesh Bharadia are with the Department of Electrical and Computer Engineering, University of California at San Diego, San Diego, CA 92093 USA (e-mail: agg003@eng.ucsd.edu; dineshb@eng.ucsd.edu).

Color versions of one or more figures in this article are available at https://doi.org/10.1109/TWC.2022.3212937.

Digital Object Identifier 10.1109/TWC.2022.3212937

this is not a scalable solution, given that spectrum is both scarce and expensive. Hence, there exists a vast literature of research on spectrum-efficient interference suppression, ranging from theoretical bounds [13], [14] to system deployments [15], [16], [17]. As Fig. 1(a) depicts, massive multiple-input multiple-output (MIMO) architectures hold the gold standard for interference suppression by digitally sampling many antennas and operating with full digital precision to alleviate interference. However, they are power-hungry and require multiple radio frequency (RF) chains for downconversion and analog-to-digital converters (ADCs) to get digital baseband samples from each antenna.

To reduce the power consumption required for interference suppression, an attractive option is to handle interference in the analog domain, referred to as analog beamforming, as shown in Fig. 1(b). In contrast to its digital counterpart, the analog beamforming approach requires a single RF chain with just one digital sampling ADC. Although the analog beamformers cut down the power requirements stemming from having multiple RF chains, they still use a phase shifter per antenna, which is often passive but introduces a high insertion loss. This high insertion loss mandates a pre-amplifying lownoise-amplifier (LNA) to offset the losses or utilize an active phase shifter with low insertion losses, both of which add to the power consumption.

To overcome the challenges articulated above, RF switches have been proposed instead of phase shifters [18], [19]. Antenna arrays employing RF switches have much lower power consumption compared to phase shifters [18] owing to the low insertion losses of RF switches while maintaining passive operation. However, RF switches offer lower flexibility in controlling the antennas in the array, as antennas can only be turned on or off. Hence, in the context of interference suppression, past work has mainly studied RF switches in a hybrid architecture [18], [20] requiring more than one RF chain. These hybrid beamformers use digital beamforming precision to improve the RF switch resolution. Other past work [19] uses a single RF chain with a switched array and combines the switch configurations across two time slots to improve the resolution. More specifically, by subtracting the residual interference terms across two time slots, [19] optimizes across $\{-1,0,1\}$ instead of $\{0,1\}$ for the switch configurations. However, this reduces the sum-rate due to using multiple time slots. Finally, due to the simplicity of RF switches, some papers in the realm of interference alignment [13] propose

1536-1276 © 2022 IEEE. Personal use is permitted, but republication/redistribution requires IEEE permission. See https://www.ieee.org/publications/rights/index.html for more information.

high signal-to-noise ratio (SNR) degrees of freedom bounds, which are theoretical in nature.

In this paper, we propose a single RF chain design with RF switches using a single time slot for interference suppression. Here, we have an integer optimization problem to determine the antenna configuration for interference suppression. We utilize a filled function approach, which changes the optimization function topology and connects the local subspaces to faroff subspaces. Hence, unlike converging to local optimizers as in prior results [19], the filled function approach creates a heuristic that converges to an approximation of the global optimum solution. Table I provides a high-level comparison between our approach using switched array antennas and prior results. Our contributions are summarized as follows:

- We propose a power-efficient interference suppression technique harnessing switch-based single-RF-chain antennas at each receiver. We assume the transmitters have no channel-state-information (CSI) and do not exchange data among themselves;
- Unlike the past work [19], which uses {-1,0,1} switch states, we focus on the binary domain, which allows us to implement the approach in a single time slot. We show via simulations that the improvement in resolution due to adding the {-1} state does not compensate for the reduction in sum-rate as a consequence of using two time slots:
- We use filled function for the antenna state optimization. This allows converging to an approximate global solution instead of a good local solution. Thus, the performance of our approach is very close to the brute force search, while having a much lower complexity;
- We also compare our optimization strategy with both phased array and digital beamforming baselines, demonstrating that our method provides higher sum-rates than phased array beamforming methods and consumes less power than digital beamforming. We evaluate our approach and the existing baselines on Rayleigh and Raytracing-based channels;
- In addition, we provide a lower bound on the minimum number of antenna elements to ensure achieving the desired signal-to-interference-plus-noise ratio (SINR) at each receiver. Moreover, we extend this result to the case when our approach uses multi-level switches.

The rest of the paper is organized as follows. In Section II, we describe our channel model and define the optimization problem. We explain our main results and proposed optimization approach in Sections III and IV, respectively. In Section V, we show a lower bound on the minimum number of antenna elements. In Section VI, we demonstrate our simulation results. Section VII describes a general lower bound on the minimum number of elements in array antenna and Section VIII concludes the paper.

II. PROBLEM SETTING AND NOTATIONS

A. Notations

We use bold-face lowercase and italic letters to denote vectors and scalars, respectively. $\mathbb{C}^{X \times 1}$ denotes the space of

 $X \times 1$ complex-valued vectors. Throughout the paper, we use calligraphic letters to denote sets. Here, $\operatorname{diag}\{\mathbf{x}\}$ represents a diagonal matrix using vector \mathbf{x} . $||\mathbf{x}||, ||\mathbf{x}||$, and \mathbf{x}^H are Euclidean norm, absolute value, and Hermitian version of complex-valued vector \mathbf{x} , respectively. \oplus denotes the summation in the binary field (XOR). We use $\mathbb{E}\left(.\right)$, $\log\left(.\right)$ to show the statistical expectation and logarithmic function in base 2, respectively. Finally, we use $\mathbf{a}.\mathbf{b}$ to describe the dot product between two vectors \mathbf{a} and \mathbf{b} .

B. Channel Model

Many end-users, such as Internet-of-Things (IoT) devices, are supposed to be simple, low-cost, and power-efficient and therefore do not have sophisticated antennas. In this work, we focus on uplink communications, and consider a single-input multiple-output (SIMO) interference channel as Fig. 2(a) where the transmitter (i.e., end-user) $\mathsf{Tx}_i, i \in \{1, 2, \dots K\}$ has a simple omni-directional antenna and receiver (i.e., BS) Rx_i is equipped with an M-element single-RF-chain antenna with a binary switch devoted to each antenna element as illustrated in Fig. 2(b).

We assume that transmitters are not aware of the CSI and only know the statistics of the channels. However, we assume Rx_i obtains its own CSI (the channel coefficients of the links connected to it) via a training phase, and beyond that, it only knows the statistics of the other channels (this assumption is referred to as the local channel state information at the receivers or local CSIR). Thus, our assumptions correspond to an interference network with no CSIT and local CSIR [23], [24]. We assume no data exchange between the transmitters, and that each receiver individually decodes its corresponding message and the receivers do not exchange any data.

In this work, we use a binary switch structure at $\mathsf{R}\mathsf{x}_i$ to enhance the performance of the network. In particular, we consider $\mathbf{s}_i\left(t\right) \in \mathcal{S}$ as the switch configuration at $\mathsf{R}\mathsf{x}_i$ at time t where $\mathbf{s}_i\left(t\right)$ is a column vector with length M and $\mathcal{S} = \{0,1\}^{M \times 1}$ is the M-tuple (s_1, s_2, \ldots, s_M) with $s_m \in \{0,1\}, m=1,2,\ldots,M$. Here, $\mathbf{h}_{ji}\left(t\right) \in \mathbb{C}^{M \times 1}$ denotes the channels between $\mathsf{T}\mathsf{x}_j$

Here, $\mathbf{h}_{ji}(t) \in \mathbb{C}^{M \times 1}$ denotes the channels between $\mathsf{T} \mathsf{x}_j$ and $\mathsf{R} \mathsf{x}_i$, $i, j \in \{1, 2, \dots K\}$ at time t. We assume $\mathbf{h}_{ji}(t)$ is a Rayleigh fading channel whose elements are distributed based on the independent and identical distribution (i.i.d.) $\mathcal{CN}\left(0, \sigma_h^2\right)$. Later, in Section VI, we use the Ray-tracing channel model to compare our method with some beamforming methods. Moreover, we consider two channel knowledge cases: (1) noiseless channels, in which $\mathsf{R} \mathsf{x}_i$ estimates its local CSIR precisely; and (2) noisy channels, where $\mathsf{R} \mathsf{x}_i$ obtains its local CSIR at SNR = p dB (noisy-p model).

Based on the above, the received signal at Rx_i is given by

$$y_{i}(t) = \left[\mathbf{s}_{i}(t) \cdot \mathbf{h}_{ii}(t)\right] x_{i}(t) + \sum_{j=1, j \neq i}^{K} \left[\mathbf{s}_{i}(t) \cdot \mathbf{h}_{ji}(t)\right] x_{j}(t) + \mathbf{s}_{i}(t) \cdot \mathbf{n}_{i}(t),$$

$$(1)$$

where $x_i\left(t\right)$ is the transmitted signal at Tx_i . We assume $\mathbb{E}\{\mathbf{x}\left(t\right)\mathbf{x}^H\left(t\right)\} = \mathrm{diag}\left(\left[P_1,P_2,\ldots,P_K\right]\right)$ where $\mathbf{x}\left(t\right) = \{x_1\left(t\right),x_2\left(t\right),\ldots,x_K\left(t\right)\}$ and $P_i,i\in\{1,2,\ldots K\}$

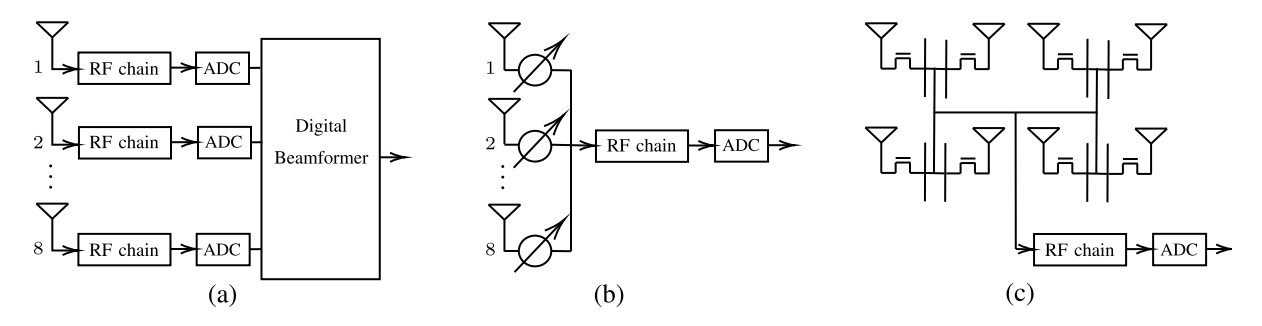


Fig. 1. (a) Massive MIMO structure; (b) Analog beamforming structure; (c) Our method with switched array antennas.

TABLE I
A COMPARISON BETWEEN OUR APPROACH WITH SWITCHED ARRAY ANTENNAS AND OTHER BEAMFORMING METHODS

Method	Beamforming	# RF Chains	Array antenna configuration	RF Front end Power Consumption	ADC Sampling Power Consumption	
[21]	Digital	>1	Digital control per antenna	Low	High	
[20]	Hybrid	>1	1-2 bits phase control	High	Medium	
[22]	Hybrid	>1	{0,1} RF Switch	Low	Medium	
[15]	Analog	1	2-4 bits phase control	High	Low	
[19]	Analog	1	{-1,0,1} RF Switch with 2 timeslots	Low	Low	
Our approach	Analog	1	{0,1} RF Switch	Low	Low	

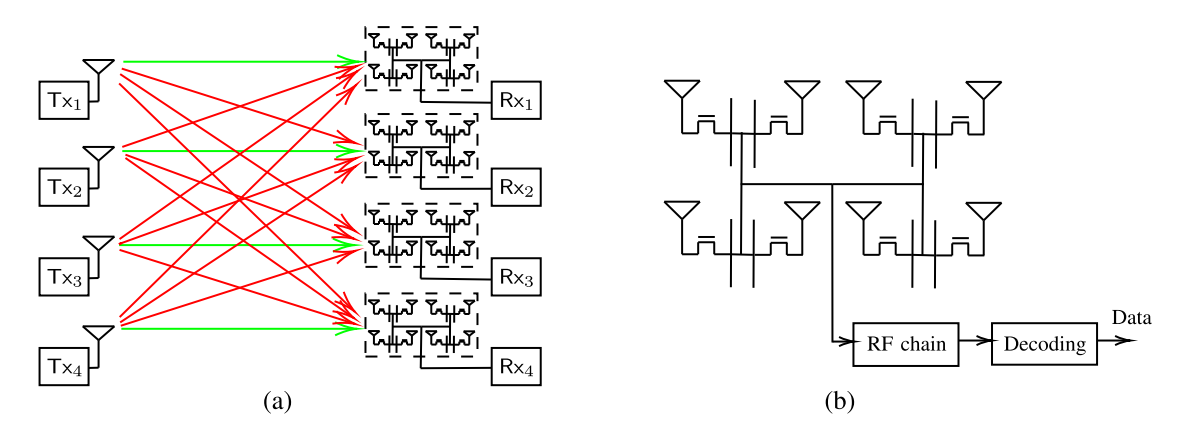


Fig. 2. (a) A 4-user interference channel where each transmitter has one antenna, and each receiver has an 8-element array antenna; (b) The structure of an 8-element array antenna at Rx_i where each element is equipped with one on/off switch.

describes the transmit power from Tx_i . Furthermore, $\mathbf{n}_i(t) \in \mathbb{C}^{M \times 1}$ represents the communication noise at Rx_i where each element of $\mathbf{n}_i(t)$ is distributed based on $\mathcal{CN}\left(0,\sigma^2\right)$. As we describe later, all operations occur in a single coherence time; thus, we will drop the time index. Finally, according to (1), we obtain the SINR at Rx_i as below:

$$SINR_i = \frac{P_{ii}|\mathbf{s}_i.\mathbf{h}_{ii}|^2}{P_{ni} + \sum_{j=1, j \neq i}^K P_{ji}|\mathbf{s}_i.\mathbf{h}_{ji}|^2},$$
 (2)

where $P_{ni} = |\mathbf{s}_i.\mathbf{n}_i|^2$ is the noise power at Rx_i . Here, $P_{ji} = P_j/d_{ji}^\alpha$ shows the received power from Tx_j at Rx_i where α is the path loss exponent and d_{ji} is the distance between Tx_j and Rx_i . We assume Rx_i learns P_{ji} 's, $j \in \{1, 2, \dots, K\}$, in a training phase before communications.

C. Optimization Problem

Characterizing the information-theoretic capacity of multiuser networks is challenging, and in fact remains open even for two-user interference channels [25], [26], [27]. Thus, similar to [18], [19], [20], [21], we focus on a more practically-feasible objective of maximizing the sum-rate. Further, as transmitters have no CSI and each receiver knows only its corresponding local CSIR, the sum-rate maximization is equivalent to individual SINR maximization, which needs to be solved individually by each receiver i for $i \in \{1, 2, ..., K\}$:

$$\max_{\mathbf{s}_{i}} \underbrace{\mathbf{SINR}_{i}}_{\mathbf{s}_{i}} \equiv \min_{\mathbf{s}_{i}} g\left(\mathbf{s}_{i}\right)$$

$$\triangleq -g(\mathbf{s}_{i})$$
s.t. $\mathbf{s}_{i} \in \mathcal{S}$, (3)

where \mathbf{s}_i is a column vector with length M that denotes the switch configuration at Rx_i and $\mathcal{S} = \{0,1\}^{M \times 1}$ represents the M-tuple (s_1, s_2, \ldots, s_M) with $s_m \in \{0,1\}, m = 1,2,\ldots,M$. The above optimization problem is a nonlinear integer programming, which is an NP-hard problem [28], and the computational complexity grows exponentially as the size

of S increases. Thus, our goal is to find an approximation of the global optimum solution for this problem.

In the next section, we present the main results of the paper.

III. MAIN RESULTS

In this section, we explain how our optimization approach performs its duty, and then we show a lower bound on the minimum number of elements in the array antenna that guarantees to achieve the desired SINR at each receiver.

A. Proposed Optimization Method

As we discussed in Section II-C, (3) is an NP-hard problem; thus, there is no efficient way of finding its optimal solution. Hence, we propose our optimization method based on a sigmoid filled function to find an approximation of the global optimum solution in (3).

In what follows, we remove index i from s_i and use sto make our optimization procedure easier to understand. To begin, we outline how an optimization method based on a general filled function executes the optimization process using local and global search methods.

1) Local Search: The goal of the local search is to find a solution that minimizes (3) locally. To describe the details, we need to define the local neighbor of s as below:

Definition 1: For any $s \in S$, local neighbor of s is

$$\mathcal{N}(s) = s \cup \{s \oplus d_m, d_m \in \mathcal{D}\},\tag{4}$$

where d_m is an M-length column vector with the m^{th} element equals to one and the others equal to zero, and D is the direction set, which is equal to $\mathcal{D} = \{d_m, m = 1, 2, \dots, M\}.$ The local search seeks to obtain $\mathbf{s}^* \in \mathcal{S}$ as the *local minimizer* of (3) if $q(\mathbf{s}^*) < q(\mathbf{s})$ for any $\mathbf{s} \in \mathcal{N}(\mathbf{s}^*)$. We call \mathbf{s}^* as a "strict local minimizer" of (3) if $g(\mathbf{s}^*) < g(\mathbf{s})$ for any $\mathbf{s} \in$ $\mathcal{N}(\mathbf{s}^*) \setminus \mathbf{s}^*$. Similarly, $\mathbf{s}^{**} \in \mathcal{S}$ is the global minimizer of (3) if $g(\mathbf{s}^{**}) \leq g(\mathbf{s})$ for any $\mathbf{s} \in \mathcal{S}$.

From now on, we use s^* to denote the local minimizer and \mathbf{s}^{**} to describe the global minimizer or the local minimizer that provides $g(\mathbf{s}^{**}) < g(\mathbf{s}^{*})$.

- 2) Global Search: The local search offers a local minimizer, which depends on the initial switch selection. In this part, we use the filled function to move from a local minimizer toward a better solution. We provide an example to describe how a general filled function intuitively leads to finding an approximation of the global optimum solution. Suppose \mathbf{s}_0^* is the local minimizer of (3) using s_0 . Here, the global search builds a filled function using $g(\mathbf{s}_0^*)$ and defines an auxiliary optimization problem (i.e., minimization problem) based on its filled function. Then, it runs the local search for the auxiliary optimization problem using \mathbf{s}_0^* to obtain $\bar{\mathbf{s}}_0^*$ as its local minimizer. Finally, it uses the local search again with the optimization problem in (3) and $\bar{\mathbf{s}}_0^*$ to obtain \mathbf{s}^{**} where $g\left(\mathbf{s}^{**}\right) < g\left(\mathbf{s}_{0}^{*}\right).$
- 3) Sigmoid Filled Function: In this paper, we use sigmoid function and propose $G_r(\mathbf{s}, \mathbf{s}^*)$, $\mathbf{s}, \mathbf{s}^* \in \mathcal{S}$ as our filled function where r > 0 is the filled function parameter and

Algorithm 1 Local Search Algorithm With s_0

```
1: \mathbf{s}^* = \mathbf{s}_0;
2: for \mathbf{d}_m \in \mathcal{D} do
         \tilde{\mathbf{s}} = \mathbf{s}_0 \oplus \mathbf{d}_m;
         if g\left(\tilde{\mathbf{s}}\right) \leq g\left(\mathbf{s}^{*}\right) then
             \mathbf{s}^* = \tilde{\mathbf{s}};
6: if \mathbf{s}^* \neq \mathbf{s}_0 then
         s_0 = s^*;
         Go to line 2;
9: else
          s^* is the local minimizer.
```

10:

 s^* denotes the current local minimizer. In this case, we define the auxiliary optimization problem as

$$\min_{\mathbf{s}} G_r(\mathbf{s}, \mathbf{s}^*)
\text{s.t.} \quad \mathbf{s}, \mathbf{s}^* \in \mathcal{S}.$$
(5)

The filled function concept was first introduced in [29] in the continuous domain. Later [30] proposed a filled function in the discrete domain. We introduce a new sigmoid filled function, compare it to the filled functions in [31] and [32], and show that our method outperforms these baselines in terms of sum-rate and complexity. We will explain the details of our optimization approach via two pseudo codes in Section IV.

B. Lower Bound on M

We provide a lower bound on the minimum number of elements in the array antenna to ensure achieving a given value of SINR_i, say SINR, at Rx_i. For this lower bound and to simplify the analysis, we assume symmetric settings where $P_{ii} = P, i, j \in \{1, 2, \dots, K\}$, and then show that in order to almost surely have $SINR_i > SINR$, we need a lower bound on M as below:

$$\begin{split} M &\geq \\ &\min_{a} \Big\{ \frac{K-1}{2} \log \Big[\frac{5P\left(K-1\right) \pi \sigma_{h}^{2} \tilde{\text{SINR}}}{P \sigma_{h}^{2} [Q^{-1} \left(\frac{1}{2^{a+1}}\right)]^{2} - 2\sigma^{2} \tilde{\text{SINR}}} \Big] + a \Big\}, \end{split} \tag{6}$$

where $Q^{-1}(.)$ is the inverse Q-function, and $0 \le a \le M$ indicates a trade-off between improving the desired signal and suppressing the interfering signal power. For example, a=0 means we use the antenna elements to reduce the interference, and a = M means that we dedicate the antenna elements to enhance the desired signal at Rx_i . We will explain the details of the lower bound in Section V.

IV. DESCRIPTION OF THE LOCAL AND GLOBAL SEARCH ALGORITHMS

A. Local Search (Phase I)

In this phase, we start with a given switch configuration and then scan all of its neighbors to obtain s^* such that $g(s^*) \le$ $g(\mathbf{s})$ for any $\mathbf{s} \in \mathcal{N}(\mathbf{s}^*)$. We present Algorithm 1 to explain the details of the local search starting from switch s_0 . We first consider $\mathbf{s}^* = \mathbf{s}_0$ since we need a switch to compare the future results with. Next, we compute $\tilde{\mathbf{s}} = \mathbf{s}_0 \oplus \mathbf{d}_m$, and if $g(\tilde{\mathbf{s}}) \leq g(\mathbf{s}^*)$, we consider $\mathbf{s}^* = \tilde{\mathbf{s}}$. We repeat lines 3 to 5 for all $\mathbf{d}_m \in \mathcal{D}$. Then, we compare \mathbf{s}^* with \mathbf{s}_0 . If they are not identical, we set $\mathbf{s}_0 = \mathbf{s}^*$ and go to line 2; otherwise, we call \mathbf{s}^* the local minimizer.

Remark 1: We note that local search finds $g(s^*)$ within a finite number of steps since there are 2^M possible solutions, which is finite.

B. Global Search (Phase II)

The global search relies on the filled function to attain an approximation of the global optimum solution. In this paper, we propose a sigmoid-based filled function with a single heuristic parameter, r, as

$$G_r\left(\mathbf{s}, \mathbf{s}^*\right) = \left(1 + \frac{1}{1 + \eta ||\mathbf{s} - \mathbf{s}^*||^2}\right) f_r\left(g\left(\mathbf{s}\right) - g\left(\mathbf{s}^*\right)\right), (7)$$

where s^* is the local minimizer of (3), (8), shown at the bottom of the next page, and

$$\eta = \begin{cases} 0, & g(\mathbf{s}) - g(\mathbf{s}^*) \le -r, \\ 1, & \text{Otherwise.} \end{cases}$$
 (9)

In Appendix A, we will enumerate the necessary conditions that a filled function must satisfy [30], and in Appendix B, we will prove that $G_r(\mathbf{s}, \mathbf{s}^*)$ in (7) meets these conditions.

High-level overview: The idea is to find a new solution that is better than \mathbf{s}_0^* , the output of the local search starting with \mathbf{s}_0 . To do this, the global search exploits two local searches based on $g(\mathbf{s})$ and $G_r(\mathbf{s},\mathbf{s}^*)$. More precisely, it uses the local search for (5) with \mathbf{s}_0^* to attain $\bar{\mathbf{s}}_0^*$ as its local minimizer. Then, it assumes $\mathbf{s}_1 = \bar{\mathbf{s}}_0^*$ and runs the local search for (3) using \mathbf{s}_1 to get \mathbf{s}_1^* . If $g(\mathbf{s}_1^*) < g(\mathbf{s}_0^*)$, we say the filled function leads to find a better solution. Otherwise, we follow the above procedure by applying the neighbors of \mathbf{s}_0^* to the filled function to find a better solution. Then, if the global search cannot find a better solution, we reduce r (i.e., r = r/10) and redo the process. The search ends if $r < \epsilon$, where ϵ is the stopping condition.

Here, to demonstrate the global search, we present a pseudo-code as Algorithm 2. We start the process by selecting r>0 and $\epsilon\ll 1$. Then, we choose switch \mathbf{s}_0 randomly and set $\ell = 0$ where ℓ describes the ℓ^{th} round of our searching algorithm. We define $r_0 = r$ to save the initial value of r. Initially, we consider $\mathbf{s}^{**} = \mathbf{s}_0$ since we need to compare $g(\mathbf{s}^{**})$ with the future outcome of our global search. Then, we run the local search for (3) with \mathbf{s}_{ℓ} to attain \mathbf{s}_{ℓ}^* as its local minimizer. Next, if $g(\mathbf{s}_{\ell}^*) < g(\mathbf{s}^{**})$, we select $\mathbf{s}^{**} = \mathbf{s}_{\ell}^*$ and set i=1 and $r=r_0$, where i describes the i^{th} neighbor of \mathbf{s}_{ℓ}^* . In line 7, we run Algorithm 1 for $G_r(\mathbf{s}_{\ell}, \mathbf{s}_{\ell}^*)$ to get $\bar{\mathbf{s}}_{\ell}^*$. If i = 1, we consider $\ell = \ell + 1$ and $\mathbf{s}_{\ell} = \bar{\mathbf{s}}_{\ell-1}^*$; otherwise, we use $\mathbf{s}_{\ell} = \bar{\mathbf{s}}_{\ell}^*$. Then, we go to line 4. We repeat lines 4 to 13 as long as $g(\mathbf{s}_{\ell}^*) < g(\mathbf{s}^{**})$. Else, if $i \leq M$, we set $\mathbf{s}_{\ell}^* = \mathbf{s}_{\ell-1}^* \oplus \mathbf{d}_i$, increase index i by one, and go to line 7. If i > M and $r \ge \epsilon$, we decrease r $(r = \frac{r}{10})$ and set i = 1 and $\ell = \ell - 1$, and go to line 7; else, we consider s^{**} as the approximation of the global minimizer.

Algorithm 2 Global Search Algorithm

1: Select r and ϵ ;

```
2: Select initial switch s_0 randomly;
 3: \ell = 0; r_0 = r; \mathbf{s}^{**} = \mathbf{s}_0;
 4: Run Algorithm 1 for (3) with \mathbf{s}_{\ell} to obtain \mathbf{s}_{\ell}^*;
 5: if g(\mathbf{s}_{\ell}^*) < g(\mathbf{s}^{**}) then
 6: \mathbf{s}^{**} = \mathbf{s}_{\ell}^{*}; i = 1;
        r=r_0;
        Run Algorithm 1 for (7) with \mathbf{s}_{\ell}^* to obtain \bar{\mathbf{s}}_{\ell}^*;
        if i=1 then
 9.
          \ell = \ell + 1;
          \mathbf{s}_{\ell} = \bar{\mathbf{s}}_{\ell-1}^*;
10:
11:
        else
12:
            \mathbf{s}_{\ell} = \bar{\mathbf{s}}_{\ell}^*;
        Go to line 4;
14: if i \leq M then
        \mathbf{s}_{\ell}^* = \mathbf{s}_{\ell-1}^* \oplus \mathbf{d}_i;
        i = i + 1;
        Go to line 7;
17:
18: else
19:
        if r \geq \epsilon then
            Decrease r; i = 1; \ell = \ell - 1;
20:
            Go to line 7;
21:
22:
            \mathbf{s}^{**} is the approximation of the global minimizer.
23:
```

V. MINIMUM NUMBER OF ELEMENTS IN ARRAY ANTENNA

In this section, we describe a lower bound on the minimum number of antenna elements to guarantee to achieve a given value of SINR_i, say SIÑR, at $Rx_i, i \in \{1, 2, ..., K\}$. To simplify the expressions, we assume a symmetric scenario where all transmitters have the same transmit power and receivers are positioned at the same distance from all transmitters (i.e., $P_{ji} = P, i, j \in \{1, 2, ..., K\}$).

To explain our analysis on M, we need the following lemma that is introduced in [19]. Here, we provide a modified version of Lemma 1 that is compatible with our binary switches.

Lemma 1: [19] If \mathbf{h}_{ji} is the channel vector between $\mathsf{T} \mathsf{x}_j$ and $\mathsf{R} \mathsf{x}_i$ whose elements are i.i.d. random variables with variance σ_h^2 , and \mathbf{s}_i is a switch whose elements are independent and drawn randomly from $\{0,1\}$, we have:

$$v\bar{a}r(\mathbf{s}_{i}.\mathbf{h}_{ji}) = \frac{M}{2}\sigma_{h}^{2},\tag{10}$$

where $var(s_i.h_{ji})$ is the average variance of $s_i.h_{ji}$.

The proof follows similar steps as the proof of Lemma 1 in [19]. The authors in [19] focus on $s_m \in \{-1,0,1\}$ and then compute $var(\mathbf{s}_i.\mathbf{h}_{ji})$, while we consider the binary switches in one time slot in this work.

We define δ_I^2 as the maximum interference power from the j^{th} unintended transmitter at Rx_i , where $i,j \in \{1,2,\ldots,K\}, j \neq i$. According to Lemma 1, $\mathbf{s}_i.\mathbf{h}_{ji}$ is distributed based on a zero-mean Gaussian distribution with variance

 $\frac{M}{2}\sigma_h^2$. Therefore, we have

$$\Pr\left(|\mathbf{s}_{i}.\mathbf{h}_{ji}| < \delta_{I}\right)$$

$$= \int_{-\delta_{I}}^{\delta_{I}} \frac{1}{\sqrt{2\pi V}} e^{-\frac{t^{2}}{2V}} dt$$

$$\stackrel{(a)}{=} \int_{-\delta_{I}}^{\delta_{I}} \frac{1}{\sqrt{2\pi V}} \left[1 - \frac{t^{2}}{2V} + \frac{t^{4}}{8V^{2}} + \dots\right] dt$$

$$= \frac{2\delta_{I}}{\sqrt{2\pi V}} + \int_{-\delta_{I}}^{\delta_{I}} \frac{1}{\sqrt{2\pi V}} \left[-\frac{t^{2}}{2V} + \frac{t^{4}}{8V^{2}} + \dots\right] dt$$

$$\stackrel{(b)}{\approx} \frac{2\delta_{I}}{\sqrt{2\pi V}} = \frac{2\delta_{I}}{\sigma_{h}\sqrt{\pi M}}, \quad j \in \{1, 2, \dots, K\}, j \neq i,$$

where $\delta_I = \max\{\delta_j = |\mathbf{s}_i.\mathbf{h}_{ji}| | j \in \{1,2,\ldots,K\}, j \neq i\}$, $V = \frac{M}{2}\sigma_h^2$, and (a) follows Taylor series expansion. In this work, our goal is to have negligible interference power, meaning δ_I should be small. Therefore, (b) holds true since the effect of the higher order terms of $\left(\frac{\delta_I}{\sqrt{V}}\right)$ is negligible. In addition, we need to meet the condition in (11) for all interfering transmitters at Rx_i . Thus, we define $\mathsf{Pr}\left(I < \delta_I\right)$ as

$$\Pr(I < \delta_I)$$

$$\triangleq \Pr(|\mathbf{s}_i.\mathbf{h}_{ji}| < \delta_I), \text{ for all } j \in \{1, 2, \dots, K\}, j \neq i. (12)$$

Moreover, we assume the channels are i.i.d. across time and users. Therefore, we have

$$\Pr(I < \delta_I) = \prod_{j \in K, j \neq i} \Pr(|\mathbf{s}_i.\mathbf{h}_{ji}| < \delta_I) \approx \left(\frac{2\delta_I}{\sigma_h \sqrt{\pi M}}\right)^{K-1}.$$
(13)

Similarly, for any $\Delta > 0$, we have

$$\Pr(|\mathbf{s}_{i}.\mathbf{h}_{ii}| > \Delta) = 2 \int_{\Delta}^{\infty} \frac{1}{\sqrt{2\pi V}} e^{\frac{-t^{2}}{2V}} dt$$
$$= 2Q\left(\frac{\Delta}{\sqrt{V}}\right) = 2Q\left(\frac{\Delta}{\sqrt{\frac{M}{2}}\sigma_{h}}\right), (14)$$

where Q(.) represents Q-function.

Finally, we provide the following lemma to show the lower bound on M that almost surely satisfies the desired SINR at Rx_i .

Lemma 2: To almost surely achieve a per-user given value of the signal-to-interference-plus-noise ratio, say SIÑR, M should satisfy the following inequality:

$$M \ge \min_{a} \left\{ \frac{K-1}{2} \log \left[\frac{5P(K-1)\pi\sigma_{h}^{2}S\tilde{INR}}{P\sigma_{h}^{2}[Q^{-1}\left(\frac{1}{2^{a+1}}\right)]^{2} - 2\sigma^{2}S\tilde{INR}} \right] + a \right\}. \tag{15}$$

Proof: Based on (13) and (14), we have $\Pr\left(I < \delta_I\right) \approx \left(\frac{2\delta_I}{\sigma_h\sqrt{\pi M}}\right)^{K-1}$ and $\Pr\left(|\mathbf{s}_i.\mathbf{h}_{ii}| > \Delta\right) = 2Q\left(\frac{\Delta}{\sqrt{\frac{M}{2}}\sigma_h}\right)$. Moreover, there are 2^M possible combinations for \mathbf{s}_i . Thus, Rx_i needs the following condition to almost surely align interference signal power and enhance its desired signal.

$$2^{M+1}Q\left(\frac{\Delta}{\sqrt{\frac{M}{2}}\sigma_h}\right)\left(\frac{2\delta_I}{\sigma_h\sqrt{\pi M}}\right)^{K-1} > 1.$$
 (16)

To calculate (16), we assume

$$\delta_I = 2^{\frac{-(M-a)}{K-1}} \sqrt{\frac{\pi M^+}{4}} \sigma_h,$$
(17)

where M^+ is the maximum possible value of M (i.e., $M < M^+$), and $0 \le a \le M$ illustrates a trade-off between improving the desired signal and suppressing the interference signals. Then, by substituting δ_I in (16), we obtain

$$2^{a+1}Q\left(\frac{\Delta}{\sqrt{\frac{M}{2}}\sigma_h}\right)\left(\frac{M^+}{M}\right)^{\frac{(K-1)}{2}} > 1,\tag{18}$$

where $\left(\frac{M^+}{M}\right)^{\frac{(K-1)}{2}} > 1$ because $M < M^+$. Thus, we need

$$Q\left(\frac{\Delta}{\sqrt{\frac{M}{2}}\sigma_h}\right) = \frac{1}{2^{a+1}},\tag{19}$$

to meet the inequality condition in (16). As a result, we calculate $\boldsymbol{\Delta}$ as

$$\Delta = \sqrt{\frac{M}{2}} \sigma_h Q^{-1} \left(\frac{1}{2^{a+1}}\right). \tag{20}$$

We note that satisfying the inequality in (16) using (17) and (20) implies that if we consider δ_I and Δ based on (17) and (20), respectively, then almost surely there exists an \mathbf{s}_i such that $|\mathbf{s}_i.\mathbf{h}_{ii}| > \Delta$ and $|\mathbf{s}_i.\mathbf{h}_{ji}| < \delta_I$ for all $j \in \{1, 2, \dots, K\}, j \neq i$.

Now, we use (2) to attain a lower bound on the SINR at Rx_i as below:

$$\begin{split} \text{SINR}_{i} &= \frac{P|\mathbf{s}_{i}.\mathbf{h}_{ii}|^{2}}{P_{ni} + P\sum_{j=1, j \neq i}^{K}|\mathbf{s}_{i}.\mathbf{h}_{ji}|^{2}} \\ &\stackrel{a.s.}{>} \frac{P\Delta^{2}}{P_{ni} + P\left(K-1\right)\delta_{I}^{2}} \stackrel{(b)}{>} \frac{P\Delta^{2}}{M\sigma^{2} + P\left(K-1\right)\delta_{I}^{2}} \\ &= \frac{P\frac{M}{2}\sigma_{h}^{2}[Q^{-1}\left(\frac{1}{2^{a+1}}\right)]^{2}}{M\sigma^{2} + P\left(K-1\right)2^{\frac{-2(M-a)}{K-1}}\frac{\pi}{4}M^{+}\sigma_{h}^{2}} \\ &> \frac{\frac{P}{2}\sigma_{h}^{2}[Q^{-1}\left(\frac{1}{2^{a+1}}\right)]^{2}}{\sigma^{2} + P\left(K-1\right)2^{\frac{-2(M-a)}{K-1}}\frac{\pi M^{+}}{4M^{-}}\sigma_{h}^{2}}, \end{split} \tag{21}$$

$$f_r\left(g\left(\mathbf{s}\right) - g\left(\mathbf{s}^*\right)\right) = \begin{cases} g\left(\mathbf{s}\right) - g\left(\mathbf{s}^*\right) + r, & g\left(\mathbf{s}\right) - g\left(\mathbf{s}^*\right) \le -r, \\ \frac{1}{1 + e^{\frac{-6}{r}\left(g\left(\mathbf{s}\right) - g\left(\mathbf{s}^*\right) + r/2\right)}}, & -r < g\left(\mathbf{s}\right) - g\left(\mathbf{s}^*\right) < 0, \\ 1, & g\left(\mathbf{s}\right) - g\left(\mathbf{s}^*\right) \ge 0, \end{cases}$$
(8)

where P_{ni} and M^- describe the noise power at Rx_i and the minimum possible value of M, respectively. Here, (a) holds true using (16). Then, (b) is obtained by using the maximum noise power.

Here, our goal is to find a lower bound on M that guarantees $\mathrm{SINR}_i \stackrel{a.s.}{>} \mathrm{SI\tilde{N}R}$. To do this, the right-hand side of (21) should be greater than or equal to $\mathrm{SI\tilde{N}R}$ as follows.

$$\frac{\frac{P}{2}\sigma_{h}^{2}[Q^{-1}\left(\frac{1}{2^{a+1}}\right)]^{2}}{\sigma^{2} + P\left(K - 1\right)2^{\frac{-2(M - a)}{K - 1}}\frac{\pi M^{+}}{4M^{-}}\sigma_{h}^{2}} \ge \tilde{SINR}.$$
 (22)

If we take \log from both sides of (22) and consider 10 < M < 100, we obtain that

$$M \ge \frac{K - 1}{2} \log \left[\frac{5P(K - 1) \pi \sigma_h^2 SI\tilde{N}R}{P \sigma_h^2 [Q^{-1} \left(\frac{1}{2^{a+1}}\right)]^2 - 2\sigma^2 SI\tilde{N}R} \right] + a.$$
(23)

We note that (23) depends on the value of $0 \le a \le M$, and M should be an integer. As a result, to calculate a lower bound on M that almost surely achieves SINR, we need

$$M \ge \min_{a} \left\{ \frac{K-1}{2} \log \left[\frac{5P(K-1)\pi\sigma_{h}^{2} \tilde{S}\tilde{I}\tilde{N}R}{P\sigma_{h}^{2}[Q^{-1}\left(\frac{1}{2^{a+1}}\right)]^{2} - 2\sigma^{2}\tilde{S}\tilde{I}\tilde{N}R} \right] + a \right\}, \tag{24}$$

and this completes the proof.

We will solve (24) numerically in Section VI. Moreover, in Section VII, we will extend these results to the case where we use multi-level switches.

We use $M_{\rm min}$ to denote the smallest integer M satisfying (24). We define "theoretical-bound" as a curve that shows the sum-rate for different values of SNR = $\frac{P}{\sigma^2}$ with respect to $M_{\rm min}$. Later, in Section VI-D, we will compare the simulation results with the theoretical-bound.

VI. NUMERICAL EVALUATION

In this section, we numerically evaluate our results. Our simulation codes are available online at [33].

The simulation results are averaged over 100 Monte-Carlo runs. Here, we use two channel models: (i) The communication channels are known perfectly, real-valued, and distributed based on Rayleigh fading. We use this channel model to evaluate the efficiency of our optimization approach, describe the lower bound on the minimum number of antenna elements, and show the complexity of our method; (ii) We use noisy and complex-valued channels generated based on the Raytracing model, which is widely used to simulate beamforming approaches [34], [35], [36], [37].

Here, we consider two types of baselines. First, we evaluate the efficiency of our optimization method and consider six different heuristic benchmarks based on a simplified exhaustive search (SES), the genetic algorithm (GA), the blind interference suppression (BIS) method [19], the successive refinement (SR) method [38], and two methods based on filled function in [31] and [32].

Second, we compare our binary switch approach with three beamforming baselines: (1) Lattice-based beamforming [20]

and WLLS [18], with finite-bit resolution at phase shifters; (2) The BIS method that uses $\{-1,0,1\}$ combining with RF switches and two time slots; (3) Fully digital beamformers with arbitrary precision from the digital domain interference suppression [21]. We also quantify the power consumption of each of these interference suppression architectures and show the power savings obtained via the switch-based approach.

Throughout this section, we use SNR = $\frac{P}{\sigma^2}$, where P is the received signal power, and σ^2 denotes the noise variance.

A. Efficiency of Our Optimization Strategy

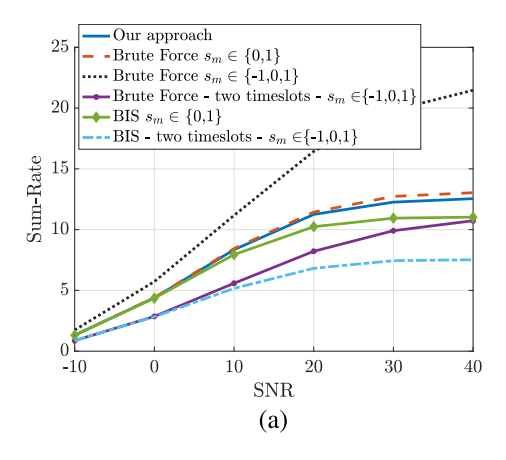
In [19], the authors present BIS, a switch-based technique that handles the interference in two consecutive time slots. Then, [19] shows that s_m can be chosen from $\{-1,0,1\}$ instead of $\{0,1\}$, which improves the RF switch resolution. However, this improvement decreases the sum-rate by 50% due to using two time slots. In Fig. 3(a), we show that the gains of using $\{-1,0,1\}$ over $\{0,1\}$ cannot compensate for the sum-rate reduction, even through the brute force method. That occurs since sending the signal in one time slot with binary switches provides better results than the BIS approach.

Although, [19] proposes a method to suppress interference in analog domain with three choices for each antenna (i.e., $\{-1,0,1\}$), it can naturally be extended to work with two choices (i.e., $\{0,1\}$) without taking a 0.5 hit in the sum-rate. Therefore, in Fig. 3(a) and (b), we compare the performance of our optimization method with the BIS method when K=4, $\sigma_h^2=1$, $\sigma^2=1$, $s_m\in\{0,1\}$, the channels are noiseless, and M=12 and 64, respectively. Here, we use $r=10^5$ and $\epsilon=10^{-4}$ in our approach. The results reveal that our method and the BIS method perform similarly if M is small; however, as M increases, our approach starts outperforming the BIS method with appreciable margins.

Next, we compare the performance of our optimization method with SES, GA, the BIS method when $s_m \in \{0,1\}$, and the SR method. We summarize how these baselines work below.

1) SES: This method defines $\mathcal{M}=\{1,2,\ldots,M\}$ as the set of antenna indices. Thereafter, it considers all subsets of \mathcal{M} that include $\hat{M}\leq M$ elements. Then, using the indices of each subset, it scans all possible corresponding switch configurations and considers the solution with the highest value of SINR to be the optimal solution. The switches whose indices are not in the subset are set to zero. In our simulations, we assume $\hat{M}=4$.

2) GA: We consider a typical GA that implements the following steps: (1) It generates ps switch configurations (parents) randomly; (2) It uses Roulette Wheel Selection to choose the optimal parents; (3) It applies the one-point cross over to the parents and then employs the bit flipping mutation technique with probability p_{μ} to generate the children. Finally, it checks the stopping condition. If the condition is not met, it goes to step 1 and repeats the process; otherwise, it considers the solution with the highest value of SINR as the optimal solution. Here, we assume ps=100, $p_{\mu}=0.1$, and stopping condition happens when the algorithm runs 100 times.



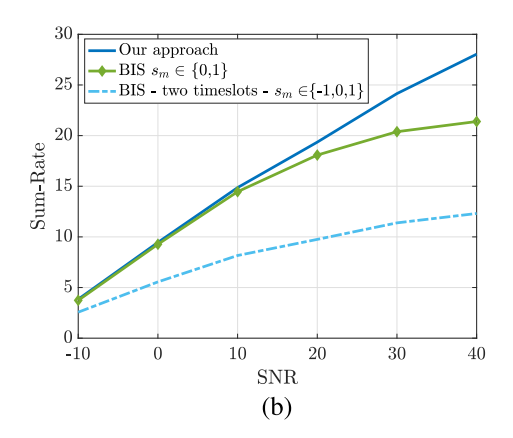


Fig. 3. (a) A comparison between our approach, two BIS methods and three brute force methods with varying switch budgets where K=4, M=12, and the channels are real-valued and distributed based on Rayleigh fading; (b) Sum-rate versus SNR with our approach and the BIS method where K=4 and M=64

3) BIS Method: This method is a combination of SES and GA. The algorithm starts with an all-zeros column vector as the initial solution. Next, it runs SES alternating \hat{M} elements and picks N_s of them as the parents, which offer the N_s maximum SINR values. Then, it fixes the values of the \hat{M} scanned switches of a given parent, and these switches will no longer be changed in the next generations of that parent. In the next iteration, for each parent, it removes the fixed indices from \mathcal{M} and runs SES for the remained indices. The algorithm ends if \mathcal{M} becomes empty. In this part, we assume $\hat{M}=2$ and $N_s=2$.

4) SR Method: In [38], the authors consider the intelligent surfaces to provide high spectrum efficiency in a power-efficient way. They propose this method to find the optimal solution when each intelligent surface utilizes a low-bit phase shifter. Due to the similarity between the optimization problem in [38] with our optimization problem, we consider the SR method as one of the baselines in this work. The SR method is an iterative algorithm that alternately optimizes each of the M switches by fixing the other M-1 switches in an iterative manner until the difference between the SINR values of two consecutive solutions is less than a threshold value. In this part, we assume the threshold is equal to 10^{-3} .

Since we use a sigmoid-based filled function to find the approximation of the global optimum solution, a logical question here is if it is possible to perform optimization using other filled functions. To answer this, we consider two different filled functions in [31] and [32] as another baselines.

Fig. 4 compares the aforementioned methods and our approach with different values of M when ${\rm SNR}=40{\rm dB}$ and the other parameters are the same as in Fig. 3. We observe that our approach performs better than BIS and GA methods, which require adjusting multiple heuristic parameters. In contrast, our approach uses r as its only heuristic parameter, and as M increases, parameter adjustments become more challenging and the gap between our approach and these methods increases. Further, our approach outperforms the SES and SR methods because these methods find the local optimal solutions. Among the benchmarks in Fig. 4, the filled function methods in [31] and [32] provide the closest performance to

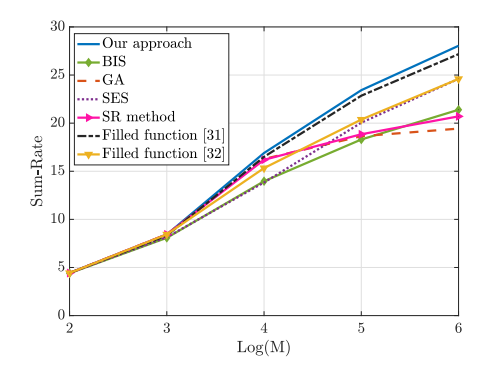


Fig. 4. A comparison between our approach, the BIS method, GA, SES, the SR method [38], and two filled function methods [31], [32] where $s_m \in \{0,1\}$, SNR = 40dB, K=4, and $M\in \{4,8,16,32,64\}$.

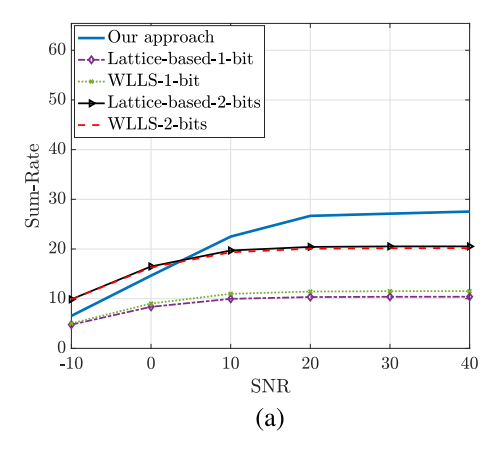
our approach as it uses a similar method. We will show later in Section VI-E that our approach has a lower complexity compared to these latter methods.

B. Our Approach Vs. Low-Bit Phase Shifters

In this part, we increase the resolution of the phase shifters at the baselines and compare the performance of our method to the beamforming techniques in [20] and [18] that use 1-bit and 2-bit phase shifters. We assume M=64, K=4, and $\sigma^2=1$ and use $r=10^5$ and $\epsilon=10^{-4}$ in our optimization method. We consider the channels are estimated at each receiver based on noisy-20 model. As Fig. 5(a) depicts, our method provides higher sum-rates compared to lattice-based beamforming and WLLS. This occurs since our method directly focuses on the discrete domain (i.e., $\{0,1\}$), while lattice-based beamforming and WLLS exploit the quantization function and determine the optimum values in the continuous domain, respectively.

C. Power Consumption

In this part, we present the comparison results between our approach and digital beamforming. In Fig. 5(b), we compare the sum-rate versus SNR with noisy-20 channels when K=4 and $M\in\{16,32,64\}$. At first glance, the results



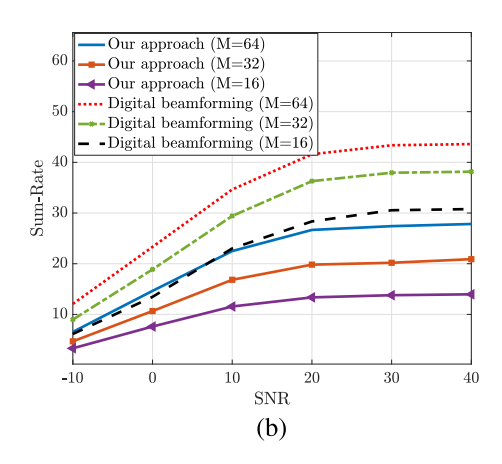


Fig. 5. (a) Sum-rate versus SNR for our approach and lattice-based beamforming and WLLS with noisy-20 channels. We assume K=4 and M=64; (b) A comparison between our approach and digital beamforming with noisy-20 channels where K=4 and $M\in\{16,32,64\}$.

in Fig. 5(b) may lead to the conclusion that digital beamforming outperforms our technique. However, Fig. 5(b) shows that our method with M=64 offers almost the same results as digital beamforming with M=16 when SNR < 20dB. Moreover, Table II demonstrates that our approach with M=64 uses 15% of the power utilized by digital beamforming with M=16 to get the identical results. We use Table III to explain how the numbers in Table II are derived. Table III presents power consumption metrics for different beamforming architectures as a function of the number of antennas and RF chains. Here, P_{PS} , P_{SW} , P_{LO} , P_{VGA} , and P_{ADC} represent the power consumption of the phase shifter, switch, local-oscillator (LO) power draw, variablegain-amplifier (VGA), and ADC, respectively. To calculate the numbers in Table II, we choose an active phase shifter with power consumption of 10mW [39], as such active vector modulator based phase shifters offer the required bit precision for interference suppression. Then, we consider P_{SW} equals to 1mW [40], since P_{SW} is around 10 times lower than P_{PS} . Finally, we use $P_{ADC} = 532.2mW, P_{LO} = 10mW$, and $P_{VGA} = 1.55mW$ [41]. As a result, according to Fig. 5(b) and Table II, our approach provides the same sum-rate as digital beamforming with lower power consumption when M = 64. We note that the results in Fig. 5(b) only apply to K-user interference channels and they may differ if we consider a broadcast channel with one BS and K users.

D. Minimum Number of Elements in the Array Antenna

To evaluate the theoretical results described in Section V, in Fig. 6(a), we show sum-rate versus SNR using our approach and the theoretical-bound. We assume K=4, $\sigma_h^2=1$, the channels are noiseless, and $\sigma^2=1$, and then use (24) to calculate $M_{\min}=24$, which almost surely ensures each receiver gets SIÑR = 16dB at SNR = 10dB. Notice that if we remove the practical interval for M and compute M numerically, then $M_{\min}=20$ is required to achieve the same performance. Therefore, in Fig. 6(a), we exhibit two curves for the theoretical-bound with K=4 and M=24, one with the practical interval for M and the other without utilizing $M^- < M < M^+$. We also take into account $r=10^5$ and

 $\epsilon=10^{-4}$ in our optimization method. Fig. 6(a) illustrates that our proposed approach provides higher sum-rates than the theoretical-bounds with the same value of M because we derive $M_{\rm min}$ pessimistically.

Then, Fig. 6(b) depicts the theoretical-bound for different values of $M_{\rm min}$. It explains that using $M_{\rm min}=128$ rather than $M_{\rm min}=64$ results in a slight improvement. Thus, we ignore the small sum-rate gain with 128 antenna elements due to the higher cost and complexity.

E. Complexity

In this part, we analyze the complexity (i.e., the number of evaluations) of our approach, brute force search and the benchmarks described in Fig. 4. We assume the symmetric settings with $P=40 \, \mathrm{dB}$, K=4, $\sigma^2=1$, $r=10^5$, $\epsilon=10^{-4}$, and noiseless real-valued Rayleigh fading channels with $\sigma_h^2=1$ when $M\in\{32,64\}$. Table IV represents the complexity of brute force search, the benchmarks mentioned in Fig. 4, and our optimization approach. We observe that our method provides a lower complexity than the two filled function-based methods and SES, which are the baselines that provide the closest sum-rate to our approach in Fig. 4. On the other hand, Fig. 4 and Table IV explain that the methods with lower sum-rate provide lower complexity, which reveals the rate-complexity trade-off of the methods.

Our goal is to obtain the solution with negligible overhead. As an example, for a carrier frequency $f_c=1.8 {\rm GHz}$ and user speed of $60 {\rm km/h}$, the coherence time equals to $c/f_c v=10 {\rm msec}$, where c denotes the speed of light. From Table IV, our method finds the solution for M=64 using a dual-core processor with a clock frequency of $2 {\rm GHz}$ in $0.06 {\rm msec}$, which is negligible.

VII. EXTENSION TO THE RESULT ON MINIMUM NUMBER OF ANTENNA ELEMENTS

In this section, we demonstrate a general lower bound on the minimum number of antenna elements when our approach utilizes multi-level switches to almost surely guarantee to achieve a given value of SINR_i, say SIÑR, at Rx_i. We consider a symmetric scenario where $P_{ji} = P$, $i, j \in \{1, 2, ..., K\}$ and

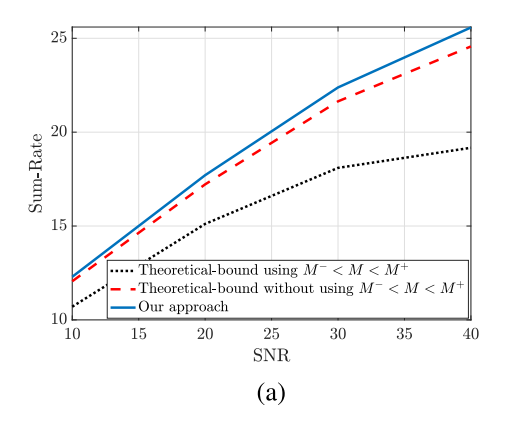
TABLE II $Power\ Consumption\ (mW)\ at\ the\ RX\ Front-End$

Architecture	Analog FE Power	LO Power	VGA Power	ADC Power	Total Power Consumption
Digital Beamforming (64 antennas, 64 RF chains)	-	640	99.4	532.3	2314.05
Digital Beamforming (16 antennas, 16 RF chains)	<u>-</u>	160	24.85	2129.2	717.45
Phased array (16 antennas, 1 RF chain)	160	10	1.55	33.3	204.85
Hybrid Switched array (16 antennas, 4 RF chains)	16	40	6.2	133.2	195.4
Switched array (64 antennas, 1 RF chain)	64	10	1.55	33.3	108.75
Switched array (16 antennas, 1 RF chain)	16	10	1.55	33.3	60.75

TABLE III

POWER CONSUMPTION FOR DIFFERENT ARCHITECTURES AS A FUNCTION OF THE NUMBER OF ANTENNAS AND RF CHAINS

Architecture	Analog FE Power	LO Power	VGA Power	ADC Power	Total Power Consumption
Digital Beamforming (M antennas, M RF chains)	-	MP_{LO}	MP_{VGA}	MP_{ADC}	$\mathbf{M}(\mathbf{P_{LO}} + \mathbf{P_{VGA}} + \mathbf{P_{ADC}})$
Phased array (M antennas, 1 RF chain)	MP_{PS}	P_{LO}	P_{VGA}	P_{ADC}	$\mathrm{MP_{PS}} + \mathrm{P_{LO}} + \mathrm{P_{VGA}} + \mathrm{P_{ADC}}$
Hybrid switched array $(M \text{ antennas}, L \text{ RF chains})$	MP_{SW}	LP_{LO}	LP_{VGA}	LP_{ADC}	$\boxed{\mathbf{MP_{SW}} + \mathbf{L}(\mathbf{P_{LO}} + \mathbf{P_{VGA}} + \mathbf{P_{ADC}})}$
Switched array (M antennas, 1 RF chain)	MP_{SW}	P_{LO}	P_{VGA}	P_{ADC}	$\mathrm{MP_{SW}} + \mathrm{P_{LO}} + \mathrm{P_{VGA}} + \mathrm{P_{ADC}}$



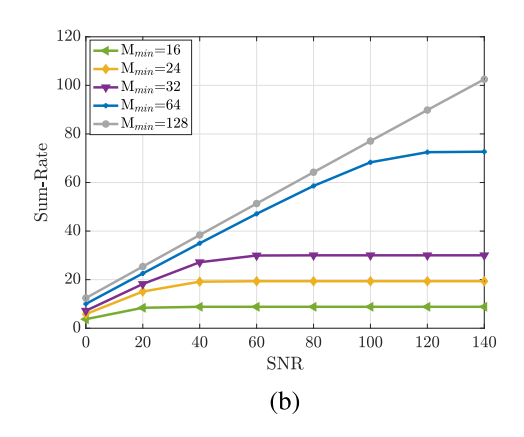


Fig. 6. (a) Sum-rate versus SNR for our proposed approach and two theoretical-bounds, one with the practical interval for M and the other without utilizing $M^- < M < M^+$, when M = 24 and K = 4; (b) The comparison between different theoretical-bounds, using (21), with different values of M_{\min} .

TABLE IV

The Complexity of Our Approach, Brute Force Search, and the Benchmarks Mentioned in Section VI-A When $P=40~dB,~K=4,~\sigma^2=1$, and Channels are Real-Valued Rayleigh With $\sigma_h^2=1$

Method	M = 32	M = 64	Method	M = 32	M = 64
Brute force	4.29×10^{9}	1.84×10^{19}	SR method	3.23×10^{4}	6.42×10^4
BIS method	2.04×10^{4}	1.69×10^{5}	Filled function in [31]	1.01×10^{5}	6.4×10^{5}
Genetic algorithm	2.01×10^{4}	2.01×10^{4}	Filled function in [32]	1.72×10^{5}	6.69×10^{5}
Simplified exhaustive search	5.39×10^{5}	9.53×10^{6}	Sigmoid filled function	6.01×10^4	2.30×10^{5}

divide interval [0,1] into $N+1, N \ge 1$ equally spaced discrete points such that $\mathbf{s}_i \in \mathcal{S}_N$ where $\mathcal{S}_N = \{0, \frac{1}{N}, \frac{2}{N}, \dots, 1\}^M$.

We note that the following lemma plays a crucial role in our analysis. Thus, we have

Lemma 3: If h_{ji} is the channel vector between $\mathsf{T}\mathsf{x}_j$ and $\mathsf{R}\mathsf{x}_i$ whose elements are i.i.d. random variables with variance σ_h^2 , and $s_i \in \mathcal{S}_N$ is a multi-level switch whose elements are independent and drawn randomly, we have:

$$v\bar{a}r(\mathbf{s}_{i}.\mathbf{h}_{ji}) = M\left(\frac{2N+1}{6N}\right)\sigma_{h}^{2}.$$
 (25)

Proof: We know

$$\operatorname{var}(\mathbf{s}_{i}.\mathbf{h}_{ji}) = \operatorname{var}\left(\sum_{m=1}^{M} s_{i,m} h_{ji,m}\right)$$

$$\stackrel{(a)}{=} \sum_{m=1}^{M} s_{i,m}^{2} \operatorname{var}(h_{ji,m}) = \sigma_{h}^{2} \sum_{m=1}^{M} s_{i,m}^{2}, (26)$$

(25) where $h_{ji,m}$ is the mth element of \mathbf{h}_{ji} and $s_{i,m} \in \{0,\frac{1}{N},\frac{2}{N},\dots,1\}$ describes the mth component of \mathbf{s}_i , and (a)

follows the fact that $s_{i,m}$ is no longer a random variable because we have all possible values of $s_{i,m}$.

Then, we consider that different configurations of \mathbf{s}_i are distributed uniformly, and obtain the average variance of $\mathbf{s}_i \cdot \mathbf{h}_{ji}$ as follows:

$$\bar{\operatorname{var}}(\mathbf{s}_{i}.\mathbf{h}_{ji}) = \mathbb{E}\left(\sigma_{h}^{2} \sum_{m=1}^{M} s_{i,m}^{2}\right) \stackrel{(b)}{=} \sigma_{h}^{2} \sum_{m=1}^{M} \mathbb{E}\left(s_{i,m}^{2}\right), \quad (27)$$

where (b) holds since $s_{i,m}$ is an i.i.d. random variable. Moreover, we know that $\mathbb{E}\left(s_{i,m}^2\right)$ is the second moment of a discrete uniform random variable $s_{i,m}$. Therefore, we have

$$\mathbb{E}\left(s_{i,m}^{2}\right) = \sum_{l \in \{0, \frac{1}{N}, \frac{2}{N}, \dots, 1\}} s_{i,m}^{2} \Pr\left(s_{i,m} = l\right)$$

$$= \frac{1}{N+1} \sum_{l \in \{0, \frac{1}{N}, \frac{2}{N}, \dots, 1\}} s_{i,m}^{2} = \frac{2N+1}{6N}. \quad (28)$$

Then, we have,

$$var(\mathbf{s}_i.\mathbf{h}_{ji}) = M\left(\frac{2N+1}{6N}\right)\sigma_h^2, \tag{29}$$

and this completes the proof.

Similar to the binary switch scenario, we can show that, for any $\delta_I > 0$, we have

$$\Pr\left(I < \delta_I\right) \approx \left(\frac{2\delta_I}{\sigma_h \sqrt{\pi M \frac{(2N+1)}{3N}}}\right)^{K-1}, \quad (30)$$

and for any $\Delta > 0$, we have

$$\Pr(|\mathbf{s}_{i}.\mathbf{h}_{ii}| > \Delta) = 2Q\left(\frac{\Delta}{\sqrt{M\left(\frac{2N+1}{6N}\right)}\sigma_{h}}\right). \tag{31}$$

Finally, we use the following lemma to derive a general description for the lower bound on M to almost surely ensure achieving the desired SINR at the intended receiver.

Lemma 4: If $\mathbf{s}_i \in \mathcal{S}_N$, $N \geq 1$, to almost surely achieve a per-user given value of the signal-to-interference-plus-noise ratio, say SINR, M should satisfy (32) (shown at the bottom of the next page), where \log_{N+1} represents logarithmic function in base N+1.

We omit the proof of Lemma 4 because it can be obtained from Lemma 2 in Section V.

According to (32), to get the same performance, if N increases, M_{\min} will decrease. For example, if $SI\tilde{N}R = 22dB$, SNR = 22dB, and K = 8, we need $M_{\min} = 48$ with $s_{i,m} \in \{0,1\}$, while we only need $M_{\min} = 19$ to get the same $SI\tilde{N}R$ if $s_{i,m} \in \{0,0.2,0.4,0.6,0.8,1\}$.

VIII. CONCLUSION

In this paper, we considered a K-user uplink interference channel and designed a low-complexity algorithmic solution for SINR maximization using a simple reconfigurable antenna with M elements. We proposed an optimization approach based on sigmoid filled function to obtain an approximation of the global optimal solution. Moreover, we provided a lower bound on the minimum number of antenna elements

to almost surely achieve a target SINR. We evaluated our approach under the Rayleigh fading and Ray-tracing channel model, and our simulation results showed that our approach outperforms other benchmarks concentrating on low-bit phase shifters. Also, our method offers almost the same results as digital beamforming while consuming less power. Considering the downlink counterpart of this work where end-users have basic antennas similar to [42], [43] would be a natural next step. Another interesting direction would be to incorporate intelligent surfaces [44], [45], [46].

APPENDIX A NECESSARY CONDITIONS OF A VALID FILLED FUNCTION

In this section, we provide the three necessary conditions of a valid filled function described in [30]. To do so, we need the following definitions.

Definition 2: [30] For any $\mathbf{s} \in \mathcal{N}(\mathbf{s})$, $\mathbf{d} \in \mathcal{D}$ is a descent direction of (3) at switch \mathbf{s} if $g(\mathbf{s} \oplus \mathbf{d}) \leq g(\mathbf{s})$. Furthermore, we call $\mathbf{d}^* \in \mathcal{D}$ as the steepest descent direction of (3) at \mathbf{s} if $g(\mathbf{s} \oplus \mathbf{d}^*) \leq g(\mathbf{s} \oplus \mathbf{d})$ for any $\mathbf{d} \in \mathcal{D}$.

Definition 3: [30] A sequence $\{s\}_{i=1}^n$ is a discrete path between any $s^{(1)} \in \mathcal{S}$ and $s^{(n)} \in \mathcal{S}$ if we have

1)
$$\mathbf{s}^{(i)} \neq \mathbf{s}^{(j)}$$
 for any $i \neq j$;
2) $||\mathbf{s}^{(2)} - \mathbf{s}^{(1)}|| = ||\mathbf{s}^{(3)} - \mathbf{s}^{(2)}||$
 $= \dots = ||\mathbf{s}^{(n)} - \mathbf{s}^{(n-1)}|| = 1.$ (33)

Moreover, we need to show that there always exists a discrete path between any two switch configurations in S. To do this, we define a discrete path connected set as below.

Definition 4: [30] A set S is defined as a discrete path connected set if, for any $\mathbf{s}^{(1)} \in S$ and $\mathbf{s}^{(2)} \in S$, there exists a discrete path between $\mathbf{s}^{(1)}$ and $\mathbf{s}^{(2)}$.

In the next section, we will show that S is a discrete path connected set. We note that the necessary conditions are built based on a discrete basin which is defined as:

Definition 5: [30] Given $\mathbf{s}^* \in \mathcal{S}$ as the local minimizer of problem (3), \mathcal{B}^* is called a discrete basin of \mathbf{s}^* if $\mathcal{B}^* \subset \mathcal{S}$ is a discrete path connected set that includes \mathbf{s}^* for which the steepest descent direction of (3) from any initial switch configuration, \mathbf{s} , converges to \mathbf{s}^* .

Here, we aim to move from \mathcal{B}^* to another basin so that the new basin helps our approach to find the global optimal solution. We call this new basin the lower basin and define it as follows:

Definition 6: [30] Given $\mathbf{s}^*, \mathbf{s}^{**} \in \mathcal{S}$ as two distinct local minimizer of problem (3) and \mathcal{B}^* and \mathcal{B}^{**} as corresponding discrete basins, respectively. We say \mathcal{B}^{**} is a lower basin than \mathcal{B}^* if $g(\mathbf{s}^{**}) < g(\mathbf{s}^*)$ and $g(\mathbf{s}') - g(\mathbf{s}^*) \leq -r$ for any $\mathbf{s}' \in \mathcal{B}^{**}$ and r > 0.

Finally, based on the above definitions, we define the conditions of a valid filled function as:

Definition 7: [30] Given s^* is a local minimizer of problem in (3) and \mathcal{B}^* as the corresponding basin. A function $G_r(s, s^*)$ is called a discrete filled function of (3) at s^* if it meets the following conditions:

 $C_1: \mathbf{s}^*$ is a strict local maximizer of $G_r(\mathbf{s}, \mathbf{s}^*)$ over S; $C_2: G_r(., \mathbf{s}^*)$ has no local minimizer in any basin \mathcal{B}' , which is higher than \mathcal{B}^* ;

 C_3 : If $G_r(s,s^*)$ has a discrete basin \mathcal{B}^{**} (corresponding to the local minimizer s^{**}) that is lower than \mathcal{B}^* (corresponding to the local minimizer s^*), there exists a switch configuration $s^{'} \in \mathcal{B}^{**}$ that minimizes $G_r(s,s^*)$ through a discrete path from s^* to s^{**} .

We will prove in Appendix B that our sigmoid filled function meets the above three conditions.

APPENDIX B PROOF OF THE FILLED FUNCTION VALIDITY CONDITIONS FOR $G_r(\mathbf{s}, \mathbf{s}^*)$

In this part, we show that our proposed filled function, $G_r(\mathbf{s}, \mathbf{s}^*)$ in (7), satisfies the three necessary conditions in Definition 7. To begin, we show that \mathcal{S} is a discrete path connected set through the following claim, and then we use a corollary to prove (\mathcal{C}_1) .

Claim 1: S defined in (3) is a discrete path connected set. Proof: Assume $\mathbf{s}^{(1)} \in \mathcal{S}$ and $\mathbf{s}^{(2)} \in \mathcal{S}$ are two arbitrary switch configurations, and there are $1 \leq \beta \leq M$ different elements between $\mathbf{s}^{(1)}$ and $\mathbf{s}^{(2)}$. Then, we use induction to prove this claim:

First, we show that the claim holds when $\beta=1$. Suppose the \mathbf{m}^{th} element of $\mathbf{s}^{(1)}$ represents the only difference between $\mathbf{s}^{(1)}$ and $\mathbf{s}^{(2)}$. In this case, we obtain $\mathbf{s}^{(2)}=\mathbf{s}^{(1)}\oplus\mathbf{d}_m$; therefore, there is no intermediate switch configuration between $\mathbf{s}^{(1)}$ and $\mathbf{s}^{(2)}$;

Second, we show that if the claim holds for β , it also holds for $\beta+1$. Assume ζ describes the path between $\mathbf{s}^{(1)}$ and $\mathbf{s}' \in \mathcal{S}$ and there are β different elements among $\mathbf{s}^{(1)}$ and \mathbf{s}' . Also, there is one different element, located at the \mathbf{m}'^{th} element of \mathbf{s}' where $1 \leq m' \leq M$, between \mathbf{s}' and $\mathbf{s}^{(2)}$. As a result, ζ and $\mathbf{d}_{m'}$ show the path between $\mathbf{s}^{(1)}$ and $\mathbf{s}^{(2)}$, and this completes the proof.

Corollary 1: (C_1) For any r > 0, s^* is a strict local maximizer of the auxiliary optimization problem in (5).

Proof: We know \mathbf{s}^* is a local minimizer of $g(\mathbf{s})$ in (3) and $g(\mathbf{s}^* \oplus \mathbf{d}) \geq g(\mathbf{s}^*)$ for any $\mathbf{d} \in \mathcal{D}$. Therefore, applying $\mathbf{s}^* \oplus \mathbf{d}$ and \mathbf{s}^* to the filled function leads to

$$G_r\left(\mathbf{s}^* \oplus \mathbf{d}, \mathbf{s}^*\right) \stackrel{(a)}{=} \frac{3}{2} < G_r\left(\mathbf{s}^*, \mathbf{s}^*\right) = 2,$$
 (34)

where (a) holds since there is only one different element between $\mathbf{s}^* \oplus \mathbf{d}$ and \mathbf{s}^* (i.e., $||(\mathbf{s}^* \oplus \mathbf{d}) - \mathbf{s}^*||^2 = 1$). Therefore, (34) proves that \mathbf{s}^* is a strict local maximizer of the auxiliary optimization problem in (5).

The following two lemmas are essential to prove (C_2) .

Lemma 5: Given that $s^* \in \mathcal{S}$ is a local minimizer of the optimization problem in (3). Assume that $s^{(1)}, s^{(2)} \in \mathcal{S}$ are two switches such that $g(s^*) \leq g(s^{(1)})$, $g(s^*) \leq g(s^{(2)})$, and $0 < ||s^{(1)} - s^*|| < ||s^{(2)} - s^*||$. Then, for any r > 0, we have

$$G_r\left(\mathbf{s}^{(2)}, \mathbf{s}^*\right) < G_r\left(\mathbf{s}^{(1)}, \mathbf{s}^*\right) < G_r\left(\mathbf{s}^*, \mathbf{s}^*\right).$$
 (35)

Proof: Since $g(\mathbf{s}^*) \leq g(\mathbf{s}^{(1)})$ and $g(\mathbf{s}^*) \leq g(\mathbf{s}^{(2)})$, we have

$$f_r\left(g\left(\mathbf{s}^{(1)}\right) - g\left(\mathbf{s}^*\right)\right) = f_r\left(g\left(\mathbf{s}^{(2)}\right) - g\left(\mathbf{s}^*\right)\right)$$
$$= f_r\left(g\left(\mathbf{s}^*\right) - g\left(\mathbf{s}^*\right)\right) = 1, \quad (36)$$

and the value of $\eta = 1$. Then, using (7) and (36), we have

$$0 < ||\mathbf{s}^{(1)} - \mathbf{s}^*|| < ||\mathbf{s}^{(2)} - \mathbf{s}^*||,$$

$$1 + \frac{1}{1 + ||\mathbf{s}^{(2)} - \mathbf{s}^*||^2} < 1 + \frac{1}{1 + ||\ textbfs^{(1)} - \mathbf{s}^*||^2} < 2,$$

$$G_r\left(\mathbf{s}^{(2)}, \mathbf{s}^*\right) < G_r\left(\mathbf{s}^{(1)}, \mathbf{s}^*\right) < G_r\left(\mathbf{s}^*, \mathbf{s}^*\right),$$
 (37)

which completes the proof.

Lemma 6: Given that $\mathbf{s}^* \in \mathcal{S}$ is a local minimizer of the optimization problem in (3). Assume $\mathbf{s}' \neq \mathbf{s}^* \in \mathcal{S}$ and $g(\mathbf{s}^*) \leq g(\mathbf{s}')$. If $g(\mathbf{s}^*) \leq g(\mathbf{s}' \oplus \mathbf{d}')$ and $||\mathbf{s}' - \mathbf{s}^*|| < ||\mathbf{s}' \oplus \mathbf{d}' - \mathbf{s}^*||$, then we have

$$G_r\left(\mathbf{s}' \oplus \mathbf{d}', \mathbf{s}^*\right) < G_r\left(\mathbf{s}', \mathbf{s}^*\right) < G_r\left(\mathbf{s}^*, \mathbf{s}^*\right).$$
 (38)

Proof: This lemma holds by Lemma 5 using $\mathbf{s}^{(2)} = \mathbf{s}' \oplus \mathbf{d}'$ and $\mathbf{s}^{(1)} = \mathbf{s}'$.

Based on Lemmas 5 and 6, we prove the second condition of a filled function as below:

Corollary 2: (C_2) $G_r(.,s^*)$ has no local minimizer in any basin \mathcal{B}' , which is higher than \mathcal{B}^* .

Proof: We provide the proof through the following: 1) From Definition 5, we know, for any $\mathbf{s}', \left(\mathbf{s}' \oplus \mathbf{d}'\right) \in \mathcal{B}'$ and $\mathbf{d}' \in \mathcal{D}$, we have $g\left(\mathbf{s}^*\right) \leq g\left(\mathbf{s}'\right)$ and $g\left(\mathbf{s}^*\right) \leq g\left(\mathbf{s}' \oplus \mathbf{d}'\right)$; 2) If $\mathbf{d}' = \mathbf{d}_m \in \mathcal{D}$ and the \mathbf{m}^{th} element of \mathbf{s}^* and \mathbf{s}' are equal, then \mathbf{d}' satisfies $||\mathbf{s}' - \mathbf{s}^*|| < ||\mathbf{s}' \oplus \mathbf{d}' - \mathbf{s}^*||$; 3) Based on Lemma 6, if $g\left(\mathbf{s}^*\right) \leq g\left(\mathbf{s}'\right)$ and $g\left(\mathbf{s}^*\right) \leq g\left(\mathbf{s}' \oplus \mathbf{d}'\right)$, then for any $\mathbf{d}' \in \mathcal{D}$ that satisfies $||\mathbf{s}' - \mathbf{s}^*|| < ||\mathbf{s}' \oplus \mathbf{d}' - \mathbf{s}^*||$, we have:

$$G_r\left(\mathbf{s}' \oplus \mathbf{d}', \mathbf{s}^*\right) < G_r\left(\mathbf{s}', \mathbf{s}^*\right) < G_r\left(\mathbf{s}^*, \mathbf{s}^*\right),$$
 (39)

where (39) shows that \mathbf{s}' is not a local minimizer of $G_r(., \mathbf{s}^*)$, and this completes the proof.

Finally, we use the following corollary to complete the validity of our sigmoid filled function.

Corollary 3: (C_3) If $G_r(s, s^*)$ has a discrete basin \mathcal{B}^{**} (corresponding to the local minimizer s^{**}) that is lower than \mathcal{B}^* (corresponding to the local minimizer s^*), there exists a switch configuration $s' \in \mathcal{B}^{**}$ that minimizes $G_r(s, s^*)$ through a discrete path from s^* to s^{**} .

Proof: According to the definition of a lower basin in Definition 6, we have:

$$g(\mathbf{s}^{**}) \stackrel{(a)}{\leqslant} g(\mathbf{s}') \stackrel{(b)}{\leqslant} g(\mathbf{s}^{*}),$$
 (40)

where (a) is true because \mathbf{s}^{**} is a local minimizer in \mathcal{B}^{**} ; (b) holds since $g(\mathbf{s}') - g(\mathbf{s}^*) \leq -r$ for any $\mathbf{s}' \in \mathcal{B}^{**}$ (i.e., $g(\mathbf{s}^{**}) - g(\mathbf{s}^{*}) \leq -r$ and $g(\mathbf{s}') - g(\mathbf{s}^{*}) \leq -r$). Therefore, we have

$$G_r\left(\mathbf{s}^{**}, \mathbf{s}^{*}\right) = 2\left(g\left(\mathbf{s}^{**}\right) - g\left(\mathbf{s}^{*}\right) + r\right)$$

$$M \ge \min_{a} \left\{ \frac{K-1}{2} \log_{N+1} \left[\frac{5P(K-1)\pi\left(\frac{2N+1}{6N}\right)\sigma_{h}^{2}SI\tilde{N}R}{P\left(\frac{2N+1}{6N}\right)\sigma_{h}^{2}\left[Q^{-1}\left(\frac{1}{2(N+1)^{a}}\right)\right]^{2} - \sigma^{2}SI\tilde{N}R} \right] + a \right\}, \tag{32}$$

$$\stackrel{(c)}{<} 2\left(g\left(\mathbf{s}'\right) - g\left(\mathbf{s}^*\right) + r\right) = G_r\left(\mathbf{s}', \mathbf{s}^*\right)$$

$$\stackrel{(d)}{<} 2 = G_r\left(\mathbf{s}^*, \mathbf{s}^*\right), \tag{41}$$

where (c) holds by (40); (d) is true because \mathbf{s}^* maximizes the auxiliary optimization problem in (5). Furthermore, we showed in Claim 1 that \mathcal{S} is a discrete path connected set. This means there exists a discrete path between \mathbf{s}^* and \mathbf{s}' , and there exists another discrete path between \mathbf{s}' and \mathbf{s}^{**} , and this completes the proof.

As a result, Corollaries 1, 2, and 3 prove that $G_r(\mathbf{s}, \mathbf{s}^*)$ in (7) is a valid filled function.

REFERENCES

- [1] L. Wang, B. Hu, and S. Chen, "Energy efficient placement of a drone base station for minimum required transmit power," *IEEE Wireless Commun. Lett.*, vol. 9, no. 12, pp. 2010–2014, Dec. 2020.
- [2] L. Bariah et al., "A prospective look: Key enabling technologies, applications and open research topics in 6G networks," *IEEE Access*, vol. 8, pp. 174792–174820, 2020.
- [3] C.-C. Lai, C.-T. Chen, and L.-C. Wang, "On-demand density-aware UAV base station 3D placement for arbitrarily distributed users with guaranteed data rates," *IEEE Wireless Commun. Lett.*, vol. 8, no. 3, pp. 913–916, Jun. 2019.
- [4] Z. Lin, M. Lin, B. Champagne, W.-P. Zhu, and N. Al-Dhahir, "Secrecy-energy efficient hybrid beamforming for satellite-terrestrial integrated networks," *IEEE Trans. Commun.*, vol. 69, no. 9, pp. 6345–6360, Sep. 2021.
- [5] P. Deyi, A. Bandi, Y. Li, S. Chatzinotas, and B. Ottersten, "Hybrid beamforming, user scheduling, and resource allocation for integrated terrestrial-satellite communication," *IEEE Trans. Veh. Technol.*, vol. 70, no. 9, pp. 8868–8882, Sep. 2021.
- [6] J. Palacios, D. Steinmetzer, A. Loch, M. Hollick, and J. Widmer, "Adaptive codebook optimization for beam training on off-the-shelf IEEE 802.11ad devices," in *Proc. 24th Annu. Int. Conf. Mobile Comput. Netw.*, Oct. 2018, pp. 241–255.
- [7] C. Li, Q. Luo, G. Mao, M. Sheng, and J. Li, "Vehicle-mounted base station for connected and autonomous vehicles: Opportunities and challenges," *IEEE Wireless Commun.*, vol. 26, no. 4, pp. 30–36, Aug. 2019.
- [8] B. Smith. (Sep. 2020). The Wireless Communications Industry and Its Carbon Footprint. [Online]. Available: https://www.azocleantech. com/article.aspx?ArticleID=1131
- [9] M. Madon. (May 2021). How to Estimate Carbon Emissions in Mobile Networks: A Streamlined Approach. [Online]. Available: https://www.ericsson.com/en/blog/2021/5/how-to-estimate-carbon-emissions-from-mobile-networks
- [10] S. Han and S. Bian, "Energy-efficient 5G for a greener future," *Nature Electron.*, vol. 3, no. 4, pp. 182–184, Apr. 2020.
- [11] W. Li, L. Tian, J. Zhang, and Y. Cheng, "Analysis of base station deployment impact on LOS probability model for 5G indoor scenario," in *Proc. IEEE/CIC Int. Conf. Commun. China (ICCC)*, Oct. 2017, pp. 1–5.
- [12] J. F. Valenzuela-Valdés, A. Palomares, J. C. González-Macías, A. Valenzuela-Valdés, P. Padilla, and F. Luna-Valero, "On the ultradense small cell deployment for 5G networks," in *Proc. IEEE 5G World Forum (5GWF)*, Jul. 2018, pp. 369–372.
- [13] S. A. Jafar, "Blind interference alignment," *IEEE J. Sel. Topics Signal Process.*, vol. 6, no. 3, pp. 216–227, Jun. 2012.
- [14] S. A. Jafar, "Interference alignment—A new look at signal dimensions in a communication network," *Found. Trends Commun. Inf. Theory*, vol. 7, no. 1, pp. 1–134, 2011.
- [15] S. Madani, S. Jog, J. O. Lacruz, J. Widmer, and H. Hassanieh, "Practical null steering in millimeter wave networks," in *Proc. 18th USENIX Symp. Netw. Syst. Design Implement.*, Apr. 2021, pp. 903–921.
- [16] S. Gollakota, S. D. Perli, and D. Katabi, "Interference alignment and cancellation," in *Proc. ACM Special Interest Group Data Commun.* (SIGCOMM), Aug. 2009, pp. 159–170.
- [17] F. Adib, S. Kumar, O. Aryan, S. Gollakota, and D. Katabi, "Interference alignment by motion," in *Proc. 19th Annu. Int. Conf. Mobile Comput. Netw. (MobiCom)*, 2013, pp. 279–290.

- [18] Z. Wang, M. Li, Q. Liu, and A. Lee Swindlehurst, "Hybrid precoder and combiner design with low-resolution phase shifters in mmWave MIMO systems," *IEEE J. Sel. Topics Signal Process.*, vol. 12, no. 2, pp. 256–269, May 2018.
- [19] M. Johnny and A. Vahid, "Low-complexity blind interference suppression with reconfigurable antennas," *IEEE Trans. Wireless Commun.*, vol. 21, no. 4, pp. 2757–2768, Apr. 2022.
- [20] S. Lyu, Z. Wang, Z. Gao, H. He, and L. Hanzo, "Lattice-based mmWave hybrid beamforming," *IEEE Trans. Commun.*, vol. 69, no. 7, pp. 4907–4920, Jul. 2021.
- [21] F. Sun and E. de Carvalho, "A leakage-based MMSE beamforming design for a MIMO interference channel," *IEEE Signal Process. Lett.*, vol. 19, no. 6, pp. 368–371, Jun. 2012.
- [22] R. Méndez-Rial, C. Rusu, N. González-Prelcic, A. Alkhateeb, and R. W. Heath, Jr., "Hybrid MIMO architectures for millimeter wave communications: Phase shifters or switches?" *IEEE Access*, vol. 4, pp. 247–267, 2016.
- [23] A. Vahid, M. A. Maddah-Ali, A. S. Avestimehr, and Y. Zhu, "Binary fading interference channel with no CSIT," *IEEE Trans. Inf. Theory*, vol. 63, no. 6, pp. 3565–3578, Jun. 2017.
- [24] A. Vahid, S.-C. Lin, and I.-H. Wang, "Erasure broadcast channels with intermittent feedback," *IEEE Trans. Commun.*, vol. 69, no. 11, pp. 7363–7375, Nov. 2021.
- [25] R. H. Etkin, D. N. C. Tse, and H. Wang, "Gaussian interference channel capacity to within one bit," *IEEE Trans. Inf. Theory*, vol. 54, no. 12, pp. 5534–5562, Dec. 2008.
- [26] A. Vahid, C. Suh, and A. S. Avestimehr, "Interference channels with rate-limited feedback," *IEEE Trans. Inf. Theory*, vol. 58, no. 5, pp. 2788–2812, May 2012.
- [27] A. Vahid, M. A. Maddah-Ali, and A. S. Avestimehr, "Capacity results for binary fading interference channels with delayed CSIT," *IEEE Trans. Inf. Theory*, vol. 60, no. 10, pp. 6093–6130, Oct. 2014.
- [28] C. W. Sung and H. Y. Kwan, "Heuristic algorithms for binary sequence assignment in DS-CDMA systems," in *Proc. 13th IEEE Int. Symp. Pers.*, *Indoor Mobile Radio Commun.*, vol. 5, Sep. 2002, pp. 2327–2331.
- [29] R. Ge, "A filled function method for finding a global minimizer of a function of several variables," *Math. Program.*, vol. 46, nos. 1–3, pp. 191–204, 1990.
- [30] C.-K. Ng, L.-S. Zhang, D. Li, and W.-W. Tian, "Discrete filled function method for discrete global optimization," *Comput. Optim. Appl.*, vol. 31, no. 1, pp. 87–115, May 2005.
- [31] Y. H. Gu and Z. Y. Wu, "A new filled function method for nonlinear integer programming problem," *Appl. Math. Comput.*, vol. 173, no. 2, pp. 938–950, Feb. 2006.
- [32] Y. M. Liang, L. S. Zhang, M. M. Li, and B. S. Han, "A filled function method for global optimization," *J. Comput. Appl. Math.*, vol. 205, no. 1, pp. 16–31, 2007.
- [33] S. Nassirpour, A. Gupta, A. Vahid, and D. Bharadia. (Mar. 2022). Simulation Codes of the Switch-Based Reconfigurable Antennas. [Online]. Available: https://github.com/SajjadNassirpour/Switch-Based-Reconfigurable-Antennas
- [34] Z. Li, S. Han, S. Sangodoyin, R. Wang, and A. F. Molisch, "Joint optimization of hybrid beamforming for multi-user massive MIMO downlink," *IEEE Trans. Wireless Commun.*, vol. 17, no. 6, pp. 3600–3614, Jun. 2018.
- [35] V. Degli-Esposti et al., "Ray-tracing-based MM-wave beamforming assessment," *IEEE Access*, vol. 2, pp. 1314–1325, 2014.
- [36] N. U. Saqib, K.-Y. Cheon, S. Park, and S.-W. Jeon, "Joint optimization of 3D hybrid beamforming and user scheduling for 2D planar antenna systems," in *Proc. Int. Conf. Inf. Netw. (ICOIN)*, Jan. 2021, pp. 703–707.
- [37] F. Fuschini, M. Zoli, E. M. Vitucci, M. Barbiroli, and V. Degli-Esposti, "A study on millimeter-wave multiuser directional beamforming based on measurements and ray tracing simulations," *IEEE Trans. Antennas Propag.*, vol. 67, no. 4, pp. 2633–2644, Apr. 2019.
- [38] Q. Q. Wu and R. Zhang, "Beamforming optimization for wireless network aided by intelligent reflecting surface with discrete phase shifts," *IEEE Trans. Commun.*, vol. 68, no. 3, pp. 1838–1851, May 2020.
- [39] H. Yan, S. Ramesh, T. Gallagher, C. Ling, and D. Cabric, "Performance, power, and area design trade-offs in millimeter-wave transmitter beamforming architectures," *IEEE Circuits Syst. Mag.*, vol. 19, no. 2, pp. 33–58, May 2019.
- [40] R. W. Heath, N. González-Prelcic, S. Rangan, W. Roh, and A. M. Sayeed, "An overview of signal processing techniques for millimeter wave MIMO systems," *IEEE J. Sel. Topics Signal Process.*, vol. 10, no. 3, pp. 436–453, Feb. 2016.

- [41] S. Dutta, C. N. Barati, D. Ramirez, A. Dhananjay, J. F. Buckwalter, and S. Rangan, "A case for digital beamforming at mmWave," *IEEE Trans. Wireless Commun.*, vol. 19, no. 2, pp. 756–770, Feb. 2020.
- [42] M. Johnny and A. Vahid, "Embedding information in radiation pattern fluctuations," in *Proc. IEEE Int. Symp. Inf. Theory (ISIT)*, Jun. 2020, pp. 1534–1539.
- [43] M. Johnny and A. Vahid, "Exploiting coherence time variations for opportunistic blind interference alignment," *IEEE Trans. Commun.*, vol. 68, no. 10, pp. 6054–6069, Oct. 2020.
- [44] S. Zhang and R. Zhang, "Capacity characterization for intelligent reflecting surface aided MIMO communication," *IEEE J. Sel. Areas Commun.*, vol. 38, no. 8, pp. 1823–1838, Aug. 2020.
- [45] X. Tan, Z. Sun, D. Koutsonikolas, and J. M. Jornet, "Enabling indoor mobile millimeter-wave networks based on smart reflect-arrays," in *Proc. IEEE INFOCOM*, Apr. 2018, pp. 270–278.
- [46] C. Huang, R. Mo, and Y. Yuen, "Reconfigurable intelligent surface assisted multiuser MISO systems exploiting deep reinforcement learning," *IEEE J. Sel. Areas Commun.*, vol. 38, no. 8, pp. 1839–1850, Jun. 2020.



Alireza Vahid (Senior Member, IEEE) received the B.Sc. degree in electrical engineering from the Sharif University of Technology, Tehran, Iran, in 2009, and the M.Sc. and Ph.D. degrees in electrical and computer engineering from Cornell University, Ithaca, NY, USA, in 2012 and 2015, respectively. From 2015 to 2017, he worked as a Post-Doctoral Research Scientist at the Information Initiative, Duke University, Durham, NC, USA. He is currently an Assistant Professor of electrical engineering at the University of Colorado at Denver, Denver, CO, USA.

His research interests include network information theory, wireless communications, coding theory, and applications of coding theory in high-performance computer memory systems. He received the 2015 Outstanding Ph.D. Thesis Research Award, the 2010 Director's Ph.D. Teaching Award, Jacobs Scholar Fellowship in 2009 from Cornell University, Qualcomm Innovation Fellowship in 2013, and the Laboratory Venture Challenge Award in 2019.



Sajjad Nassirpour (Graduate Student Member, IEEE) received the B.Sc. degree in electrical engineering from Shiraz University, Shiraz, Iran, in 2011, and the M.Sc. degree in electrical engineering from the Iran University of Science and Technology, Tehran, Iran, in 2014. He is currently pursuing the Ph.D. degree with the Department of Electrical Engineering, University of Colorado Denver, Co, USA. His research interests include network information theory, wireless communications, machine learning, and applications of coding theory

in high-performance computer memory systems. He has received the Best Paper Award at the IEEE Computing and Communication Workshop and Conference (CCWC) in 2020.



Agrim Gupta (Student Member, IEEE) received the B.Tech. and M.Tech. degrees (Hons.) from the Indian Institute of Technology Bombay in 2019. He is currently pursuing the Ph.D. degree with the University of California at San Diego (UCSD) with the WCSNG Research Group headed by Prof. Dinesh Bharadia. His research interests include low-power wireless sensing, wireless localization, and MIMO systems. He received the Undergraduate Research Award for his thesis work on MIMO-OFDM precoding.



Dinesh Bharadia (Member, IEEE) received the bachelor's degree in electrical engineering from the Indian Institute of Technology, Kanpur, in 2010, and the Ph.D. degree from the Electrical Engineering Department, Stanford University. His Ph.D. thesis invalidated a long-held assumption in wireless communication by building full-duplex radios. From 2013 to 2015, he was a Principal Scientis with Kumu Networks, where he worked to commercialize his research on full-duplex radios, building a product that underwent successful field trials at

Tier 1 network providers worldwide like Deutsche Telekom and SK Telecom. He is currently an Assistant Professor at the UC San Diego, where he leads the Wireless Communication Sensing and Networking Group (WCSNG). His research interests include inter-disciplinary advancing the theory and design of modern wireless communication and sensing systems and low-power networks. In recognition of his research, he was named as a Marconi Young Scholar for Outstanding Wireless Research and awarded the Michael Dukkakis Leadership Award. He was also named as one of the top 35 innovators under 35 in the world by MIT Technology Review in 2016 and worldwide Forbes 30 under and 30 for Science category in 2018. He was a recipient of the Stanford Graduate Fellowship and a Gold Medal at the IIT Kanpur for graduating at the top of his class.